Strain-mediated Giant Magnetoelectric Coupling in a Crystalline Multiferroic Heterostructure

Adrián Begué[†,‡] and Miguel Ciria[*,†,‡]

†*Instituto de Nanociencia y Materiales de Aragón (INMA), CSIC-Universidad de Zaragoza, Spain.*

‡*Departamento de Física de la Materia Condensada, Universidad de Zaragoza, Zaragoza, Spain.*

E-mail: miguel.ciria@csic.es

Abstract

Multiferroic heterostructures based on the strain-mediated mechanism present ultra-low heat dissipation and large magnetoelectric coupling coefficient, two conditions that require endless improvement for the design of fast nonvolatile random access memories with reduced power consumption. This work shows that a structure consisting of a $[Pb(Mg_{1/3}Nb_{2/3})O_3]_{0.7}$-$[PbTiO_3]_{0.3}$ (001) substrate on which a crystalline MgO(001)/FeGa(001) bilayer is deposited exhibits a giant magnetoelectric coupling coefficient of order $15 \times 10^{-6} sm^{-1}$ at room temperature. That result is a twofold increment over the previous highest value. The spatial orientation of the magnetization vector in the epitaxial FeGa film is switched 90^o with the application of electric field. The symmetry of the magnetic anisotropy is studied by the angular dependence of the remanent magnetization demonstrating that poling the sample generates a switchable uniaxial magnetoelastic anisotropy in the film that overcomes the native low fourfold

magnetocrystalline anisotropy energy. Magnetic force microscopy shows that the switch of the easy axis activates the displacement of domain walls and the domain structure remain stable after that point. This result highlights the interest in single crystalline structures including materials with large magnetoelastic coupling and small magnetocrystalline anisotropy for low-energy consuming spintronic applications.

Keywords

Multiferroics, magneto-elastic coupling, piezo-strain, electrical magnetization switching, epitaxial FeGa

1 Introduction

The processing of information requires very efficient devices with low-energy consumption, a goal that is hampered if electric current is used to switch non-volatile states.[1,2] This request has motivated the evolution of the vintage idea of a material with interconnected magnetic and electric capacities[3] into sophisticates magnetoelectric (ME) heterostructures encompassing components with enhanced ferroelectric (FE) and ferromagnetic (FM) properties.[4–7] For the latter structures, the ME coupling strength can be three or more orders of magnitude[8–10] higher than that for single-phase materials[11,12] and the active control of the magnetic state by the FE part of the structure can be easily achieved at room temperature.[13] Several mechanisms are capable of controlling the magnetization M without magnetic field or electric current.[9,14–16] One of them is based on the strain transferred from the FE crystal to a FM film, which generates an uniaxial magnetic anisotropy through the magnetoelastic coupling effect.[17–19] Other mechanisms are based on phenomena located at the FE-FM interface: modification of the population of spin-up and spin-down electron density of states[20] and voltage-driven oxygen migration and modification of the oxide ferromanget.[21] The strain-transfer mechanism shows lower heat dissipation per switching cycle[16] and presents larger

magnetoelectric coupling parameter α_E than any other coupling mechanism.[9]

Materials with large electrostriction, as the relaxor FE compound $[Pb(Mg_{1/3}Nb_{2/3})O_3]_{(1-x)}$-$[PbTiO_3]_x$ (x $\sim$ 0.3) (PMN-PT),[22] are used to induce strain in magnetic thin films with significant magnetoelastic coupling. Many of these films are amorphous[17,23] or polycrystalline[24–29] to diminish the native large magnetocrystalline anisotropy that can conceal the effect due to the FE domain switching, usually detected by 90^o easy axis switching.[30] Studies on crystalline films presents also strain induced effects[8,31–34] and dependencies of the cubic magneto-crystalline constants with E.[35,36] However, the larger values of α_E for strain-mediated coupling are below 10^{-5} sm^{-1}.[9,10,29]

This work reports on a hybrid ME structure including a crystalline layer of the magnetostrictive FeGa alloy that presents values for α_E in the range of 10^{-5} sm^{-1} at room temperature. This result is achieved by the activation of a uniaxial magnetoelastic anisotropy on top of the native small cubic magnetocrystalline anisotropy. The crystalline magnetoelectric structure is obtained by the deposition of a thin layer of MgO (001) on a PMN-PT(001) substrate as a buffer layer. The $Fe_{100-z}Ga_z$ alloy, with z around 20, has been proposed as magnetic component in ME devices to achieve the switching between defined magnetic states.[37] The reason is the giant tetragonal magnetostriction,[38,39] which can reach a value more than 50 times that of pure iron with appropriate doping.[40] The cubic magnetocrystalline energy in $Fe_{80}Ga_{20}$ is small with values for the first order anisotropy coefficient K_1 around -10 kJm^{-3},[41,42] clearly below that the value for pure iron of 48 kJm^{-3}. The change in the sign of K_1 means that for (001) thin films the easy axis moves from the <100> to the <110> directions as the gallium content increases. Thus, FeGa crystalline films with intrinsic small cubic magnetic anisotropy and large magnetostriction can improve the performances of magnetoelectronic devices based on converse magnetoelectric mechanisms.

2 Results and discussion

The multiferroic heterostructure consists of a PMN-PT(001) FE substrate, coated with a crystalline MgO(001) seed layer ($\approx$ 3 nm in thickness) for a FeGa(001) magnetic layer approximately 15 nm in thickness and a Mo overcoat 2 nm thick. The Mo/FeGa/MgO trilayer was grown by molecular beam epitaxy. The crystal orientation of these layers is observed *in situ* by Reflection High Energy Electron Diffraction (RHEED), and *ex situ* by aberration-corrected scanning transmission electron microscopy. The resulting epitaxial relationships are: FeGa[110] $\parallel$ MgO[100] $\parallel$ PMN-PT[100], and FeGa[100] $\parallel$ MgO[110] $\parallel$ PMN-PT[110] (for details of the film growing and its characterization see Supporting Information).

Figure 1a shows MH loops of the as-grown film carried out by Vibrating Sample Magnetometry (VSM) with H applied along the [100] and [110] FeGa directions. These loops suggest the presence of a fourfold magnetic anisotropy (see Supporting Information). It is observed that the magnetic behavior FE-FM systems can be inhomogeneous due to the presence of several switching modes.[43,44] Thus, the measurement of the magnetic response of the whole film averages the variation of M under the application of E causing a decrement in α_E. In order to avoid this effect the magnetic behavior of the film is measured employing a MOKE magnetometer with a laser focus spot diameter in the micrometer range. Figure 1b displays the Kerr rotation signal for loops taken on the as-grown film, that serve as reference for the effect of poling the FE crystal. The loop with H along the [001] direction show features that can be explained by the presence of quadratic contributions to the Kerr rotation (see Supporting Information). The azimuth dependence of the remanent magnetization obtained from the MOKE measurements normalized by the signal at the saturation field, $S_K(\varphi)$, is presented in Figure 1c as function of the φ angle between **H** and the FeGa [100] direction. The symmetry of this curve can be associated with a dominant fourfold anisotropy term in the film plane. Also, assigning the easy (hard) directions with high (low) S_K determines that the [110] direction is the easy axis (EA) and the [100] one the hard axis (HA), a fact also observed in FeGa films with similar composition grown directly on MgO(100) crystals.[42]

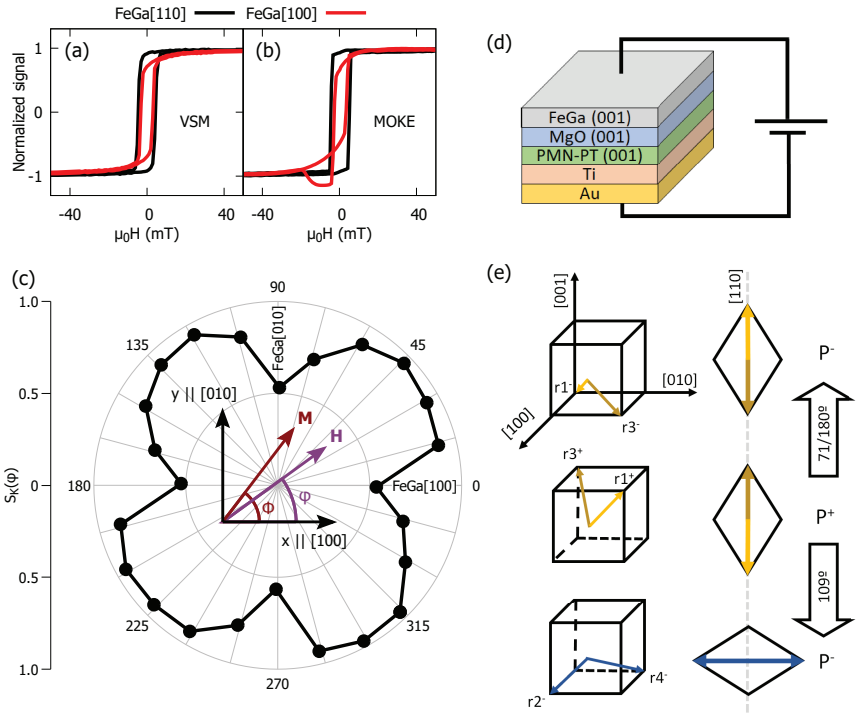

Figure 1: Hysteresis loops for the as-grown FeGa(100) film performed by means of (a) VSM magnetometry and (b) Kerr magnetometry. The magnetic field is applied along the [110] and [100] in-plane directions. The magnetic signals were normalized by the value obtained at saturation at 100 mT. (c) Polar plot of the angular dependence of the Kerr signal obtained at remanence normalized by the saturation value $S_K(\varphi)$. The coordinate system and the angle definition used in the text is shown as inset. (d) Schematic drawing of the device fabricated to apply electric field. (e) Sketch of the ferroelectric switching mechanisms with E applied along the [001] direction.

In order to apply electric field along the [001] direction of the PMN-PT(001) crystal, a Ti/Au bilayer was deposited on the uncovered PMN-PT surface (Figure 1d). An initial poling of the crystal was performed by application of $E = 0.6$ MVm^{-1}. The symbols 0+ and 0- are used to define the state of remanent polarization after applying electric field with positive and negative polarity, respectively, and $|E| = 0.3$ MVm^{-1} which is large enough to switch **P** (Figure 1e). Kerr loops were performed at several areas of the film to identify the homogeneity of the magnetic behavior in the sample.[43] The most compelling result is shown in Figure 2a and b, where Kerr rotation loops with H along the FeGa [100] and [010] directions for 0+ and 0- states are compared. These loops demonstrate that the EA and HA switched 90^o by the action of **E**. Notice also that S_k for the HA loop abates when compared with the value obtained from the HA loop taken before poling (Figure 1b). These results indicate that the uniaxial magnetic anisotropy emerged with the application of **E** can be controlled externally. However, for other regions of the film the configuration of easy and hard direction remains fixed under the application of electric field with positive or negative bias. The inhomogeneous magnetic response of the FeGa film has been also observed in amorphous CoFeB thin films[43] and mesoscopic disc.[44] In any case, the change in the magnetic behavior requests new magnetic anisotropies to explain the observed behavior.

The S_K *vs* E dependency shown in Figure 2c was obtained from Kerr rotation loops (see Supporting Information) performed with H applied along the FeGa [100] direction at fixed values of E. The large jumps of $S_K(E)$ observed for $E \sim 0.15$ MVm^{-1} and $E \sim$ -0.1 MVm^{-1} present an asymmetry with respect to E. An explication for the shift in the $S_K(E)$ curve could be ascribed to the inhomogeneous FE domain switching through the structure. The ferromangetic exchange coupling interaction across the boundary of areas with switchable and fixed EA favors parallel orientation of M. The effect of this interaction is an unidirectional anisotropy that can enforce or arrest the inversion of **M** in the reversible area and is observed as a shift of the $S_K(E)$ loop.

The converse magnetoelectric coupling coefficient α_E, calculated from the $S_K(E)$ data

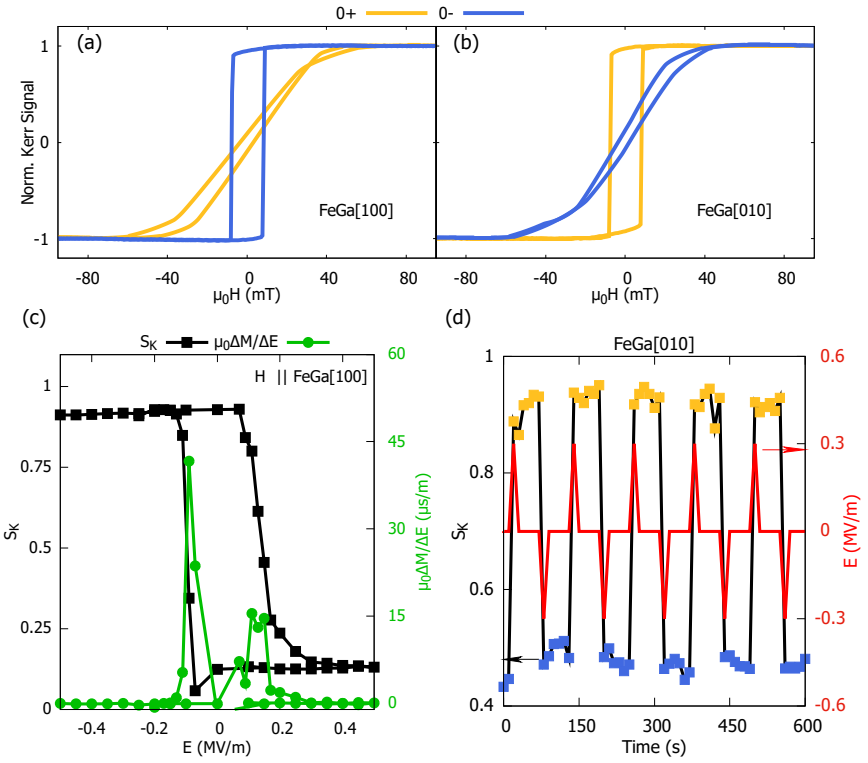

Figure 2: Hysteresis loops for the FeGa(100) film obtained by means of MOKE magnetometry in the film at 0 Vm^{-1} after applying positive (0+) and negative (0-) electric field. The magnetic field is applied along (a) [100] and (b) [010] FeGa directions. (c) Variation of S_K and magnetoelectric coupling coefficient with the electric field. (d) Normalized Kerr rotation signal vs time curve showing 5 cycles of repeatable high and low magnetization states switched by pulses of electric field.

as $\mu_0 \Delta M/\Delta E$ (μ_0 is the vacuum permeability), is also shown in Figure 2c. The value of α_E around E = 0.15 MVm^{-1} is 15 $\times$ 10^{-6} sm^{-1}, and is, up to our knowledge the largest α_E observed for any kind of coupling mechanism:[9,10] α_E of order 8 $\times$ 10^{-6} sm^{-1} is obtained for optimized structures of amorphous films grown on relaxor substrates,[10] while for oxide magnetic layers α_E can be of order 10^{-7} sm^{-1}.[8] For the interfacial oxidation coupling mechanism α_E decreases to values in the range of 10^{-8} sm^{-1}.[9] We note that $\alpha_E \sim$ 40 $\times$ 10^{-6} sm^{-1} at E = -0.1 MVm^{-1}, although the switching rate can be enhanced by the orientation of M in neighbor domains. The Kerr loops used to calculate α_E were obtained in an area with EA switching. In other regions the maxima of α_E could peak at different E or have smaller magnitude because the Kerr signal integrates the response from domains that switch at different values of E (see Supporting Information).

A large change in the value of $S_K(\varphi)$ at specific values of φ can be useful for applications. An important issue is the observation of reproducible changes in the magnetic response through the application of pulses of E with alternating polarity. Figure 2d has been obtained at H = 0 mT after saturating the film along a direction close to one FeGa [010] axis in the area that shows EA switching; it presents repeatable jumps between two clearly different values, for a set of 10 pulses with $|E|$ = 0.3 MVm^{-1}. The Kerr rotation signal changes markedly and abruptly when the electric field pulse oscillates between positive and negative values back and forth. It is relevant that the magnitude of the switching between two states is large and around a fixed value. 180^o switching, from +M to -M,[45] can also be obtained with the assistance of external magnetic field of 3 mT (see the Supporting Information).

$S_K(\varphi)$ illustrates the modification of the magnetic energy landscape occurring with the application of electric field. To avoid the incertitude in the Kerr signal due to the location of the laser spot during the rotation on an inhomogeneous FE substrate, the angular position of the magnetic field is modified by the use of a quadrupole magnet.[46] (see Supporting Information) The resulting polar plots of $S_K(\varphi)$ for the 0+ and 0- states are shown in Figure 3a. These curves displays a clear twofold symmetry, obvious differences with respect to the

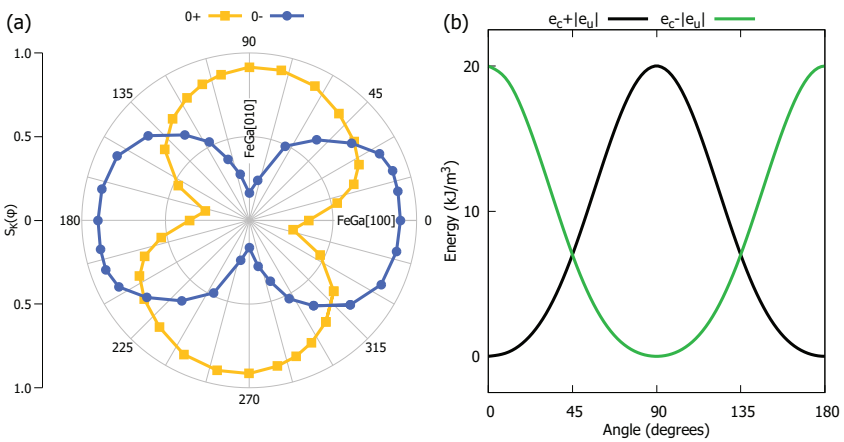

Figure 3: (a) Squareness versus φ angle for the 0- and 0+ states obtained by rotation the H with a quadrupole magnet. (b) Sum of the unixial $e_u = K_{me} sin^2\phi$ and cubic anisotropy energies $e_c = K_1 \sin^2\phi \cos^2\phi$ as function of the azimuth angle for $|K_{me}/K_1| = 1.67$, the minimum and maximum shift 90^o by changing the sign of K_{me}.

fourfold $S_K(\varphi)$ data obtained before poling the substrate, and demonstrate the switching of 90 ^{o} between easy and hard directions by the application of E.

Active control of magnetic domain walls (DW's)[47–50] is a matter of interest for practical applications.[51] Magnetic force microscopy is used to directly observe the displacement and stability of the magnetic domain structure under the application of electric field without the presence of magnetic field except for that emanating from the tip. The starting magnetic domain structure was obtained from a 0+ state with the application of magnetic field along the hard direction. Figure 4a shows the magnetic image with contrast due to the presence of DW's since M lays in the film plane. Figure 4b was taken at E = -0.08 MVm^{-1}, which is around the value for which a large jump of $S_K(E)$ is observed (Figure 2c). Compared with image of Figure 4a clear changes are present at E = -0.08 MVm^{-1}: sets of lines appear in areas without features while some DW's do not move but others disappear. The increment of the magnetic contrast of the film, with lines and other features on the whole area, could indicate as non-homogeneous switching of $\mathbf{P}$ which causes misalignment of $\mathbf{M}$, also in a non-homogeneous fashion, by the stresses arisen from the FE domains. Increasing the strength of E to -0.14 MVm^{-1}, see Figure 4c, changes the landscape of the domain structure to a configuration that remains stable for E = -0.2 MVm^{-1} (Figure 4d) as well as for the 0- state

(Figure 4e). For this set of three images only minor changes are observed in the geometry and position of the DW's probably induced by the magnetic tip. A second application of E with positive bias (0+ state) modifies the domain configuration as is shown in Figure 4.f. However, the domain configuration of the 0+ states (Figure 4.a and 4.f) share the presence of domain walls quite parallel to the easy axis as those at the bottom left corner close to the white arrow.

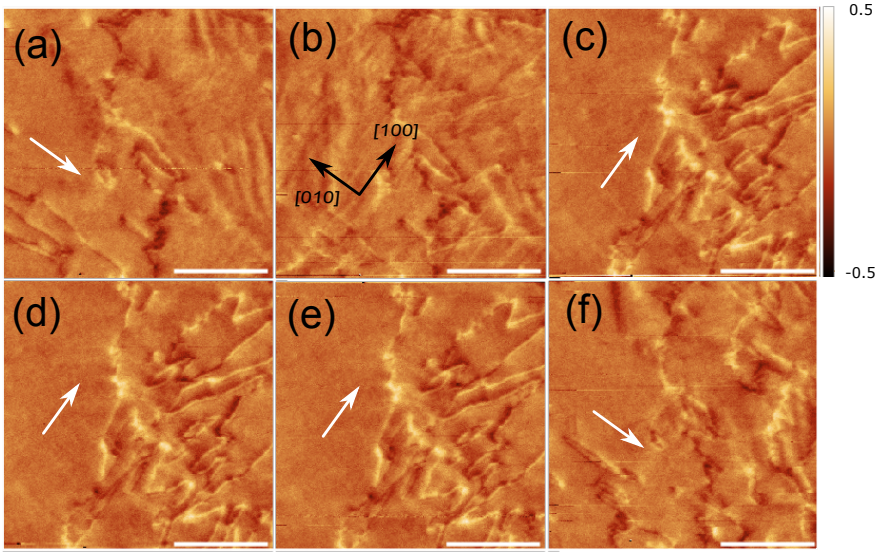

Figure 4: Magnetic force microscopy images taken on the film at different values of electric field on the same area: (a) 0+, (b) -0.08 MV/m, (c) -0.14 MV/m, (d) -0.2 MV/m, (e) 0- and (f) 0+. The arrows in panel b stand for the FeGa [100]/[010] in-plane directions. The white arrows indicate the magnetic easy axis. The units of color code bar are degrees. Scale bar length 10 μm.

2.1 Analysis

The angular dependencies of $S_K(\varphi)$ presented in Figure 1c and 3a suggest the activation of an uniaxial anisotropy contribution that overcomes the cubic anisotropy term. The strain-induced magnetoelastic contribution is the only term consider here, and the magnetic energy density, with the assumption that $\mathbf{M}$ lies on the film plane, can be written as $e(\phi) = K_1 \sin^2\phi\cos^2\phi - B_1(\epsilon_{xx} - \epsilon_{yy})\sin^2\phi + B_2\epsilon_{xy}\sin 2\phi$ (see Supporting Information). The Cartesian reference system is aligned with the <100> directions of the FeGa layer with z

parallel to the film normal and ϕ the angle between $\mathbf{M}$ and the [100] direction. B_1 and B_2 are cubic magnetoelastic stress coefficients and ϵ_{xx}, ϵ_{yy} and ϵ_{xy} in-plane strain components which are induced by the PMN-PT substrate.

The switching of $\mathbf{P}$ between different <111> directions by the application of $\mathbf{E}$ on the PMN-PT(001) crystal along the [001] direction can be achieved by several modes (Figure 1e) that causes an asymmetric butterfly-like strain versus E curve.[52] The ferroelectric switching of $\mathbf{P}$ by the 109^o mechanism provides ferroelastic jumps that persists at remanence with a value of order 0.04%[52] for the strain along {110} directions. However, the mixture of the switching modes (109^o with 71^o and 180^o mechanisms) in the whole substrate can translate the strain to the film with values that fluctuate[17,52,53] and modify locally the magnetic anisotropy coefficients.[54] The proportion of polarization variants with 109^o switching varies in crystals with the same nominal composition.[52] Thus, the observation of areas with induced uniaxial anisotropy insensitive to the bias of the electric field is compatible with FE domains undergoing 71^o and 180^o switching modes (see Figure 1e).

The combination of Kerr and scanning electron microscopy with polarization analysis (SEMPA) measurements has linked the shape of $S_K(\varphi, E)$ to the presence of single or multidomain ferroelectric switching.[44] In mesoscopic amorphous CoFeB discs the rotation of 90^o of both $\mathbf{M}$, observed directly by SEMPA, and $S_K(\varphi)$, measured by Kerr effect, are ascribed to the 109^o domain switching of a single variant. $S_K(\varphi)$ for the FeGa film rotates by 90^o between the 0- and 0+ states, see Figure 3.a., in agreement with the data reported for CoFeB amorphous discs.[44] This result suggests that in the zone probed by the Kerr magnetometer a single FE variant undergoes a 109^o switching. Thus, ΔM_r and α_E can be ascribed to the activation of a uniaxial magnetic anisotropy originated in that single domain area.

Because the FeGa[100] directions are parallel to the PMN-PT[110] crystal axes, the in-plane shear distortion of the FE domains is transmitted to the FeGa(001) plane as a rectangular distortion of the square symmetry of the FeGa film along the [100] and [010] directions, with strain components $\epsilon_{xx} = -\epsilon_{yy}$ and $\epsilon_{xy} = 0$. Thus, the uniaxial strain-induced magnetic

anisotropy is $K_{me}\sin^2\phi$, with $K_{me} = 2B_1\epsilon_{xx}$. Getting $\epsilon_{xx} = \pm 0.04$ % and $B_1 \approx$ -15 MPa[38,39] (for $Fe_{80}Ga_{20}$) $|K_{me}| = 12$ kJm^{-3} with the sign coefficient oscillating from positive to negative as the rectangular distortion $\epsilon_{xx} - \epsilon_{yy}$ does.

The value of K_1 is estimated from the MH loops as the energy required to saturate the film along [100] and [110] direction. Thus, taking $\mu_0 M_s = 1.65$ T for $Fe_{80}Ga_{20}$,[39] the value $K_1 \approx$ -12 kJm^{-3} is obtained. The HA loops in Figure 2a are used to obtain for the unixial anisotropy constant of order 20 kJm^{-3} (using for the anisotropy field $\mu_0 H_a = 2M_s K_u \approx 30$ mT), which is not far form the value calculated above. Managing $e(\phi)$ with $\epsilon_{xy} = 0$, it can be easily shown that the minima of $e(\phi)$ depends on the ratio K_{me}/K_1. For $|K_{me}/K_1| > 1$ the maxima and minima are at $\phi = 0 + n\pi$ (n is an integer). Therefore, using $|K_{me}| =$ 20 kJm^{-3}, and K_1= -12 kJm^{-3}, the $e(\phi)$ curves obtained for $\pm K_{me}$ are shown in Figure 3b observing that the maxima/minima are exchanged between [100] and [010] directions as function of the sign of K_{me}, in agreement with the experimental results.

3 Conclusions

A crystalline multiferroic structure with giant value for α_E of order 15×10^{-6}sm^{-1} is obtained in a full crystalline heterostructure at room temperature. The heterostructure consists of a PMN-PT(001) FE substrate, coated with a crystalline MgO(001) seed layer ($\approx$ 3 nm in thickness) for a FeGa magnetic layer approximately 15 nm in thickness and a Mo overcoat 2 nm thick. The alignment of the [100]FeGa with [110]PMN-PT determines that the uniaxial easy/hard directions switches between [100] and [010] FeGa directions with the application of electric field along the [001] direction. The rectangular distortion of the square symmetry of the FeGa film acts as driving factor to activate the magnetoelastic uniaxial energy. This contribution overcomes the cubic anisotropy observed in the as-grown structure, before the initial poling of the PMN-PT crystal.

The experimental procedure used to obtain the multiferroic heterostructure presented

here was not optimized to maximize the value of α_E, but was used to demonstrate the effect of incorporating a crystalline magnetostrictive layer. Thus, it can be foreseen that systematic studies varying preparation conditions can improve largely the strength α_E in multiferroic heterostructures with magnetic crystalline layers, a fundamental issue to design devices for low-energy magnetic memory technologies.

Acknowledgement

This work was supported by Spanish MICINN (Grant No. MAT2015-66726-R), and Aragón Government (Grant E10-17D) and Fondo Social Europeo. A.B. acknowledges funding from Ministry of Science and Innovation Ph. D. contract No BES-2016-076482. We thank Dr. A. Ibarra for the assistance in STEM measurements. The authors thank Servicio General de Apoyo a la Investigación-SAI (Universidad de Zaragoza), Laboratorio de Microscopías Avanzadas (Universidad de Zaragoza) and Servicio de Caracterización de Superficies y Recubrimientos (CEQMA) for the use of NanoMoke, STEM and AFM/MFM facilities.

Supporting Information Available

The following files are available free of charge.

- Supplementary Information: methods; Heterostructure growth and structural characterization (RHEED, STEM and AFM measurements); additional data and discussions about MOKE and VSM experiments; demonstration of 180^o switching of $\mathbf{M}$ with the assistance of magnetic field and the derivation of the magnetic anisotropy energy.

References

(1) Matsukura, F.; Tokura, Y.; Ohno, H. Control of Magnetism by Electric Fields. *Nat. Nanotechnol.* **2015**, *10*, 209–220.

(2) Bandyopadhyay, S.; Atulasimha, J. *Nanomagnetic and Spintronic Devices for Energy-Efficient Memory and Computing*, 1st ed.; Wiley, 2016.

(3) Curie, P. Sur la Symétrie dans les Phénomènes Physiques, Symétrie d'un Champ Électrique et d'un Champ Magnétique. *J. Physique (3rd series)* **1894**, *3*, 393–415.

(4) Fiebig, M. Revival of the Magnetoelectric Effect. *J. Phys. D: Appl. Phys.* **2005**, *38*, R123–R152.

(5) Spaldin, N. A.; Fiebig, M. The Renaissance of Magnetoelectric Multiferroics. *Science* **2005**, *309*, 391–392.

(6) Eerenstein, W.; Mathur, N. D.; Scott, J. F. Multiferroic and Magnetoelectric Materials. *Nature* **2006**, *442*, 759–765.

(7) Bibes, M.; Barthélémy, A. Towards a Magnetoelectric Memory. *Nat. Mater.* **2008**, *7*, 425–426.

(8) Eerenstein, W.; Wiora, M.; Prieto, J. L.; Scott, J. F.; Mathur, N. D. Giant Sharp and Persistent Converse Magnetoelectric Effects in Multiferroic Epitaxial Heterostructures. *Nat. Mater.* **2007**, *6*, 348–351.

(9) Hu, J.-M.; Duan, C.-G.; Nan, C.-W.; Chen, L.-Q. Understanding and Designing Magnetoelectric Heterostructures Guided by Computation: Progresses, Remaining Questions, and Perspectives. *npj Comput. Mater.* **2017**, *3*, article no 18.

(10) Wang, J.; Pesquera, D.; Mansell, R.; van Dijken, S.; Cowburn, R. P.; Ghidini, M.; Mathur, N. D. Giant Non-Volatile Magnetoelectric Effects Via Growth Anisotropy in $Co_{40}Fe_{40}B_{20}$ Films on PMN-PT Substrates. *Appl. Phys. Lett.* **2019**, *114*, article no 092401.

(11) Folen, V. J.; Rado, G. T.; Stalder, E. W. Anisotropy of the Magnetoelectric Effect in Cr_2O_3. *Phys. Rev. Lett.* **1961**, *6*, 607–608.

(12) Hur, N.; Park, S.; Sharma, P. A.; Ahn, J. S.; Guha, S.; Cheong, S.-W. Electric Polarization reversal and Memory in a Multiferroic Material Induced by Magnetic Fields. *Nature* **2004**, *429*, 392–395.

(13) Heron, J. T.; Bosse, J. L.; He, Q.; Gao, Y.; Trassin, M.; Ye, L.; Clarkson, J. D.; Wang, C.; Liu, J.; Salahuddin, S.; Ralph, D. C.; Schlom, D. G.; Iñiguez, J.; Huey, B. D.; Ramesh, R. Deterministic Switching of Ferromagnetism at Room Temperature Using an Electric Field. *Nature* **2014**, *516*, 370–373.

(14) Song, C.; Cui, B.; Li, F.; Zhou, X.; Pan, F. Recent Progress in Voltage Control of Magnetism: Materials, Mechanisms, and Performance. *Prog. Mater Sci.* **2017**, *87*, 33 – 82.

(15) Meisenheimer, P. B.; Novakov, S.; Vu, N. M.; Heron, J. T. Perspective: Magnetoelectric Switching in Thin Film Multiferroic Heterostructures. *J. Appl. Phys.* **2018**, *123*, article no 240901.

(16) Hu, J.-M.; Nan, C.-W. Opportunities and Challenges for Magnetoelectric Devices. *APL Mater.* **2019**, *7*, article no 080905.

(17) Zhang, S.; Zhao, Y. G.; Li, P. S.; Yang, J. J.; Rizwan, S.; Zhang, J. X.; Seidel, J.; Qu, T. L.; Yang, Y. J.; Luo, Z. L.; He, Q.; Zou, T.; Chen, Q. P.; Wang, J. W.; Yang, L. F.; Sun, Y.; Wu, Y. Z.; Xiao, X.; Jin, X. F.; Huang, J.; Gao, C.; Han, X. F.; Ramesh, R. Electric-Field Control of Nonvolatile Magnetization in $Co_{40}Fe_{40}B_{20}/Pb(Mg_{1/3}Nb_{2/3})_{0.7}Ti_{0.3}O_3$ Structure at Room Temperature. *Phys. Rev. Lett.* **2012**, *108*, article no 137203.

(18) Kim, J.-Y.; Yao, L.; van Dijken, S. Coherent Piezoelectric Strain Transfer to Thick Epitaxial Ferromagnetic Films with Large Lattice Mismatch. *J. Phys.: Condens. Matter* **2013**, *25*, article no 082205.

(19) Bhattacharya, D.; Bandyopadhyay, S.; Atulasimha, J. Voltage Induced Strain Control of Magnetization: Computing and other Applications. *Multifunct. Mater.* **2019**, *2*, article no 032001.

(20) Duan, C.-G.; Velev, J. P.; Sabirianov, R. F.; Zhu, Z.; Chu, J.; Jaswal, S. S.; Tsymbal, E. Y. Surface Magnetoelectric Effect in Ferromagnetic Metal Films. *Phys. Rev. Lett.* **2008**, *101*, article no 137201.

(21) Bauer, U.; Yao, L.; Tan, A. J.; Agrawal, P.; Emori, S.; Tuller, H. L.; van Dijken, S.; Beach, G. S. D. Magneto-ionic Control of Interfacial Magnetism. *Nat. Mater.* **2015**, *14*, 174–181.

(22) Thiele, C.; Dörr, K.; Bilani, O.; Rödel, J.; Schultz, L. Influence of Strain on the Magnetization and Magnetoelectric Effect in $La_{0.7}A_{0.3}MnO_3$/PMN-PT(001)(A=Sr,Ca). *Phys. Rev. B* **2007**, *75*, article no 054408.

(23) Lou, J.; Reed, D.; Pettiford, C.; Liu, M.; Han, P.; Dong, S.; Sun, N. X. Giant Microwave Tunability in FeGaB/Lead Magnesium Niobate-Lead Titanate Multiferroic Composites. *Appl. Phys. Lett.* **2008**, *92*, 16–19.

(24) Wu, T.; Bur, A.; Wong, K.; Zhao, P.; Lynch, C. S.; Amiri, P. K.; Wang, K. L.; Carman, G. P. Electrical Control of Reversible and Permanent Magnetization Reorientation for Magnetoelectric Memory Devices. *Appl. Phys. Lett.* **2011**, *98*, article no 262504.

(25) Brandlmaier, A.; Geprägs, S.; Woltersdorf, G.; Gross, R.; Goennenwein, S. T. B. Nonvolatile, Reversible Electric-Field Controlled Switching of Remanent Magnetization in Multifunctional Ferromagnetic/Ferroelectric Hybrids. *J. Appl. Phys.* **2011**, *110*, article no 043913.

(26) Nan, T.; Zhou, Z.; Liu, M.; Yang, X.; Gao, Y.; Assaf, B. A.; Lin, H.; Velu, S.; Wang, X.; Luo, H.; Chen, J.; Akhtar, S.; Hu, E.; Rajiv, R.; Krishnan, K.; Sreedhar, S.; Heiman, D.;

Howe, B. M.; Brown, G. J.; Sun, N. X. Quantification of Strain and Charge co-mediated Magnetoelectric Coupling on Ultra-Thin Permalloy/PMN-PT Interface. *Sci. Rep.* **2014**, *4*, article no 3688.

(27) Shen, J.; Cong, J.; Chai, Y.; Shang, D.; Shen, S.; Zhai, K.; Tian, Y.; Sun, Y. Nonvolatile Memory Based on Nonlinear Magnetoelectric Effects. *Phys. Rev. Applied* **2016**, *6*, article no 021001.

(28) Zhang, S.; Chen, Q.; Liu, Y.; Chen, A.; Yang, L.; Li, P.; Ming, Z. S.; Yu, Y.; Sun, W.; Zhang, X.; Zhao, Y.; Sun, Y.; Zhao, Y. Strain-mediated Coexistence of Volatile and Nonvolatile Converse Magnetoelectric Effects in $Fe/Pb(Mg_{1/3}Nb_{2/3})_{0.7}Ti_{0.3}O_3$ Heterostructure. *ACS Appl. Mater. Interfaces* **2017**, *9*, 20637–20647.

(29) Jahjah, W.; Jay, J.-P.; Le Grand, Y.; Fessant, A.; Prinsloo, A.; Sheppard, C.; Dekadjevi, D.; Spenato, D. Electrical Manipulation of Magnetic Anisotropy in a $Fe_{81}Ga_{19}/Pb(Mg_{1/3}Nb_{2/3})O_3$-$Pb(Zr_xTi_{1-x})O_3$ Magnetoelectric Multiferroic Composite. *Phys. Rev. Applied* **2020**, *13*, article no 034015.

(30) Buzzi, M.; Chopdekar, R. V.; Hockel, J. L.; Bur, A.; Wu, T.; Pilet, N.; Warnicke, P.; Carman, G. P.; Heyderman, L. J.; Nolting, F. Single Domain Spin Manipulation by Electric Fields in Strain Coupled Artificial Multiferroic Nanostructures. *Phys. Rev. Lett.* **2013**, *111*, article no 027204.

(31) Yang, J. J.; Zhao, Y. G.; Tian, H. F.; Luo, L. B.; Zhang, H. Y.; He, Y. J.; Luo, H. S. Electric Field Manipulation of Magnetization at Room Temperature in Multiferroic $CoFe_2O_4/Pb(Mg_{1/3}Nb_{2/3})_{0.7}Ti_{0.3}O_3$ Heterostructures. *Appl. Phys. Lett.* **2009**, *94*, article no 212504.

(32) Lee, Y.; Liu, Z. Q.; Heron, J. T.; Clarkson, J. D.; Hong, J.; Ko, C.; Biegalski, M. D.; Aschauer, U.; Hsu, S. L.; Nowakowski, M. E.; Wu, J.; Christen, H. M.; Salahuddin, S.;

Bokor, J. B.; Spaldin, N. A.; Schlom, D. G.; Ramesh, R. Large Resistivity Modulation in Mixed-phase Metallic Systems. *Nat. Commun.* **2015**, *6*, article no 5959.

(33) Guo, X.; Han, X.; Zuo, Y.; Zhang, J.; Li, D.; Cui, B.; Wu, K.; Yun, J.; Wang, T.; Peng, Y.; Xi, L. Electric Field Induced Magnetic Anisotropy Transition from Fourfold to Twofold Symmetry in (001) 0.68 $Pb(Mg_{1/3}Nb_{2/3})O_3-0.32PbTiO_3/Fe_{0.86}B_{0.14}$ Epitaxial Heterostructures. *Appl. Phys. Lett.* **2016**, *108*, article no 152401.

(34) Guo, X.; Zuo, Y.; Li, D.; Cui, B.; Wu, K.; Yun, J.; Wang, T.; Xi, L. Electrical Field Control of Non-volatile 90^o Magnetization Switching in Epitaxial FeSi Films on (001) $0.7[Pb(Mg_{1/3}Nb_{2/3})O_3]-0.3[PbTi_{0.3}O_3]$. *Appl. Phys. Lett.* **2016**, *108*, article no 042403.

(35) Zhou, C.; Shen, L.; Liu, M.; Gao, C.; Jia, C.; Jiang, C. Strong Nonvolatile Magnon-driven Magnetoelectric Coupling in Single-crystal $Co/[PbMg_{1/3}Nb_{2/3}O_3]_{0.71}[PbTiO_3]_{0.29}$ Heterostructures. *Phys. Rev. Applied* **2018**, *9*, article no 014006.

(36) Zhou, C.; Shen, L.; Liu, M.; Gao, C.; Jia, C.; Jiang, C.; Xue, D. Long-range Nonvolatile Electric Field Effect in Epitaxial $Fe/Pb(Mg_{1/3}Nb_{2/3})_{0.7}Ti_{0.3}O_3$ Heterostructures. *Adv. Funct. Mater.* **2018**, *28*, article no 1707027.

(37) Hu, J.-M.; Li, Z.; Chen, L.-Q.; Nan, C.-W. High-density Magnetoresistive Random Access Memory Operating at Ultralow Voltage at Room Temperature. *Nat. Commun.* **2011**, *2*, article no 553.

(38) Clark, A. E.; Restorff, J. B.; Wun-Fogle, M.; Lograsso, T. A.; Schlagel, D. L. Magnetostrictive Properties of Body-Centered Cubic Fe-Ga and Fe-Ga-Al Alloys. *IEEE Trans. Magn.* **2000**, *36*, 3238–3240.

(39) Clark, A. E.; Wun-Fogle, M.; Restorff, J.; Lograsso, T.; Cullen, J. Effect of Quenching on the Magnetostriction on $Fe_{1-x}Ga_x$ ($0.13<x<0.21$). *IEEE Trans. Magn.* **2001**, *37*, 2678–2680.

(40) Yangkun, H.; Xiaoqin, K.; Chengbao, J.; Naihua, M.; Hui, W.; David, C. J. M.; Yunzhi, W.; Huibin, X. Interaction of Trace Rare-Earth Dopants and Nanoheterogeneities Induces Giant Magnetostriction in Fe-Ga Alloys. *Adv. Funct. Mater.* **2018**, *28*, article no 1800858.

(41) Rafique, S.; Cullen, J. R.; Wuttig, M.; Cui, J. Magnetic Anisotropy of FeGa Alloys. *J. Appl. Phys.* **2004**, *95*, 6939–6941.

(42) Begué, A.; Proietti, M. G.; Arnaudas, J. I.; Ciria, M. Magnetic Ripple Domain Structure in FeGa/MgO Thin Films. *J. Magn. Magn. Mater.* **2020**, *498*, article no 166135.

(43) Li, P.; Zhao, Y.; Zhang, S.; Chen, A.; Li, D.; Ma, J.; Liu, Y.; Pierce, D. T.; Unguris, J.; Piao, H.-G.; Zhang, H.; Zhu, M.; Zhang, X.; Han, X.; Pan, M.; Nan, C.-W. Spatially Resolved Ferroelectric Domain-Switching-Controlled Magnetism in $Co_{40}Fe_{40}B_{20}/Pb(Mg_{1/3}Nb_{2/3})_{0.7}Ti_{0.3}O_3$ Multiferroic Heterostructure. *ACS Appl. Mater. Interfaces* **2017**, *9*, 2642–2649.

(44) Ba, Y.; Liu, Y.; Li, P.; Wu, L.; Unguris, J.; Pierce, D. T.; Yang, D.; Feng, C.; Zhang, Y.; Wu, H.; Li, D.; Chang, Y.; Zhang, J.; Han, X.; Cai, J.; Nan, C.-W.; Zhao, Y. Spatially Resolved Electric-field Manipulation of Magnetism for CoFeB Mesoscopic Discs on Ferroelectrics. *Adv. Funct. Mater.* **2018**, *28*, article no 1706448.

(45) Zhang, S.; Zhao, Y.; Xiao, X.; Wu, Y.; Rizwan, S.; Yang, L.; Li, P.; Wang, J.; Zhu, M.; Zhang, H.; Jin, X.; Han, X. Giant Electrical Modulation of Magnetization in $Co_{40}Fe_{40}B_{20}/Pb(Mg_{1/3}Nb_{2/3})_{0.7}Ti_{0.3}O_3$ (011) Heterostructure. *Sci. Rep.* **2015**, *4*, article no 3727.

(46) Li, J.; Jin, E.; Son, H.; Tan, A.; Cao, W. N.; Hwang, C.; Qiu, Z. Q. Design of a Vector Magnet for the Measurements of Anisotropic Magnetoresistance and Rotational Magneto-Optic Kerr Effect. *Rev. Sci. Instrum.* **2012**, *83*, article no 033906.

(47) Chung, T.-K.; Carman, G. P.; Mohanchandra, K. P. Reversible Magnetic Domain-wall Motion under an Electric Field in a Magnetoelectric Thin Film. *Appl. Phys. Lett.* **2008**, *92*, article no 112509.

(48) Lahtinen, T. H. E.; Franke, K. J. A.; van Dijken, S. Electric-field Control of Magnetic Domain Wall Motion and Local Magnetization Reversal. *Sci. Rep.* **2012**, *2*, article no 258.

(49) Parkes, D. E.; Cavill, S. A. T., S. A.. andCavill; Wadley, P.; McGee, F.; Staddon, C. R.; Edmonds, K. W.; Campion, R. P.; Gallagher, B. L.; Rushforth, A. W. Non-Volatile Voltage Control of Magnetization and Magnetic Domain Walls in Magnetostrictive Epitaxial Thin Films. *Appl. Phys. Lett.* **2012**, *101*, article no 072402.

(50) Lei, N.; Devolder, T.; Agnus, G.; Aubert, P.; Daniel, L.; Kim, J.-V.; Zhao, W.; Trypiniotis, T.; Cowburn, R. P.; Chappert, C.; Ravelosona, D.; Lecoeur, P. Strain-controlled Magnetic Domain Wall Propagation in Hybrid Piezoelectric/Ferromagnetic Structures. *Nat. Commun.* **2013**, *4*, article no 1378.

(51) Parkin, S. S. P.; Hayashi, M.; Thomas, L. Magnetic Domain-wall Racetrack Memory. *Science* **2008**, *320*, 190–194.

(52) Yang, L.; Zhao, Y.; Zhang, S.; Li, P.; Gao, Y.; Yang, Y.; Huang, H.; Miao, P.; Liu, Y.; Chen, A.; Nan, C. W.; Gao, C. Bipolar Loop-like Non-volatile Strain in the (001)-oriented $Pb(Mg_{1/3}Nb_{2/3})O_3$-$PbTiO_3$ Single Crystals. *Sci. Rep.* **2014**, *4*, article no 4591.

(53) Qiao, K.; Wang, J.; Hu, F.; Li, J.; Zhang, C.; Liu, Y.; Yu, Z.; Gao, Y.; Su, J.; Shen, F.; Zhou, H.; Bai, X.; Wang, J.; Franco, V.; Sun, J.; Shen, B. Regulation of Phase Transition and Magnetocaloric Effect by Ferroelectric Domains in FeRh/PMN-PT Heterojunctions. *Acta Mater.* **2020**, *191*, 51 – 59.

(54) Lo Conte, R.; Xiao, Z.; Chen, C.; Stan, C. V.; Gorchon, J.; El-Ghazaly, A.; Nowakowski, M. E.; Sohn, H.; Pattabi, A.; Scholl, A.; Tamura, N.; Sepulveda, A.;

Carman, G. P.; Candler, R. N.; Bokor, J. Influence of Nonuniform Micron-scale Strain Distributions on the Electrical Reorientation of Magnetic Microstructures in a Composite Multiferroic Heterostructure. *Nano Lett.* **2018**, *18*, 1952–1961.

Graphical TOC Entry